American Mineralogist, Volume 88, pages 639–646, 2003

Trace-element partitioning between apatite and carbonatite melt

STEPHAN KLEMME† AND CLAUDE DALPÉ‡

Department of Earth Sciences, University of Bristol, Bristol BS8 1RJ, U.K.

ABSTRACT

To establish more fully a basis for quantifying the role of apatite in trace-element fractionation processes, hitherto unknown mineral/melt partition coefficients ($D^{apatite/melt}$) for a variety of trace elements (Li, Be, B, K, Cs, Rb, Ba, Th, U, Nb, Ta, La, Ce, Sr, Pr, Hf, Zr, Sm, Gd, Y, Lu, and Pb) have been measured between fluorapatite [$Ca_5(PO_4)_3F$], chlorapatite [$Ca_5(PO_4)_3Cl$], and hydroxylapatite [$Ca_5(PO_4)_3OH$] and carbonatite melt.

Apatites were equilibrated experimentally with carbonatite melts at 1 GPa and 1250 °C, and run products were analyzed for trace elements by secondary ion mass spectrometry (SIMS) and by laser ablation inductively coupled plasma-mass spectrometry (LA-ICP-MS). Calculated partition coefficients indicate incompatibility of most analyzed elements. Rare-earth element (REE) partition coefficients show a convex-upward pattern, indicating that apatite prefers the middle (Sm, Gd) relative to the lighter (La, Ce, Pr) and heavier REE (Lu).

Comparison of partition coefficients determined in this study with previous results in silicate systems reveals a strong influence of melt chemistry on partition coefficients, namely decreasing partition coefficients with decreasing silica-content, and increasing Ca and P in melts.

INTRODUCTION

Apatite [$Ca_5(PO_4)_3(F,Cl,OH)$] is an ubiquitous accessory phase in a wide range of igneous, metamorphic, and sedimentary rocks. Because of its capacity to incorporate significant concentrations of geochemically important minor and trace elements, apatite is among the most important minerals in controlling rare-earth element (REE) variations in igneous rocks (Watson and Green 1981; Harrison and Watson 1984; Hoskin et al. 2000). Apatite is very common in carbonatites (cf., Hogarth 1989; Seifert et al. 2000; Bühn et al. 2001), in some cases so abundant that certain carbonatites are important P ores (cf., Eriksson 1989; Zaitsev and Bell 1995). Despite its petrogenetic importance, however, there is surprisingly little experimental data as to how trace elements partition between apatite and silicate melts (e.g., Watson and Green 1981; Green 1994). Moreover, there are no published experimental partition coefficients between apatite and carbonatite melt.

Apatite has frequently been reported from metasomatized mantle xenoliths in a number of locations world-wide and, therefore, is potentially an important reservoir of halogens, REE, and P in the Earth's mantle (Frey and Green 1974; Yaxley et al. 1991; Haggerty et al. 1994; Ionov et al. 1993, 1994, 1997; Matsumoto et al. 1997; Yaxley et al. 1998; Yaxley and Kemenetsky 1999; Coltorti et al. 1999; O'Reilly and Griffin 2000). If precipitated from a carbonatite melt in the Earth's mantle (e.g., Green and Wallace 1988; Yaxley et al. 1991), apatite may play an important role in mantle metasomatism on a global scale (Green and Wallace 1988; Yaxley et al. 1991; Baker and Wyllie 1992; Klemme et al. 1995; Yaxley et al. 1998). Furthermore, apatite is likely to be the host for P during recycling of sediments in subduction zones, as subducted sediments contain significant amounts of P (e.g., Sorensen and Grossman 1993, Plank and Langmuir 1998). Sediment melting during subduction (Plank and Langmuir 1993; Nichols et al. 1994; Elliott et al. 1997; Rosenbaum et al. 1997) is a viable mechanism for refertilizing the Earth's mantle in terms of P. However, there is very little information as to what the fate of subducted P-bearing and carbonate-rich sediments is, but early experimental studies (Biggar 1966; see also Boettcher et al. 1980) seemed to suggest that primary melts derived from these sediments are broadly "carbonatitic" in nature. Under these circumstances, apatite may, as a residual accessory phase, play a key role in controlling the trace-element budget of melts formed from subducted sediments.

Watson and Green (1981) reported a significant influence of bulk composition on measured mineral/melt trace element partition coefficients between apatite and a variety of silicate melts ($D^{apatite/melt}$). Their data indicated strongly decreasing $D^{apatite/melt}$ with decreasing silica activity of the melt. One of the aims of the present study was to test trends observed by Watson and Green (1981) and investigate trace-element partitioning between apatite and carbonatite melt, i.e., with a melt with very low silica activity. Furthermore, a

* E-mail: sklemme@min.uni-heidelberg.de
† Current address: University of Heidelberg, Mineralogical Institute, Im Neuenheimer Feld 236, 69120 Heidelberg, Germany.
‡ Current address: Royal Canadian Mounted Police, Forensic Laboratory Services, 1200 Vanier Parkway, Ottawa, ON K1A OR2, Canada

0003-004X/03/0004–639$05.00

similar influence of melt composition on trace-element partition coefficients also has been suggested by Blundy and Dalton (2000), who found somewhat different trace-element partitioning between clinopyroxene and silicate and carbonatite melt, respectively.

To address the aforementioned matters, partition coefficients between apatite and carbonatite melts were determined experimentally at high pressures and high temperatures.

Experimental and analytical techniques

Experimental rationale

Phase relations between apatite and carbonatitic melts at high pressures and high temperatures are not well understood. Biggar (1966) studied parts of the system CaO-MgO-P_2O_5-H_2O up to 0.2 GPa; Ryabchikov et al. (1991) and Baker and Wyllie (1992) investigated the solubility of apatite in carbonatitic melts in complex compositions. There is clearly a lack of systematic experimental studies investigating differentiation of phosphate-bearing carbonatitic melts. The present study was performed on the joins $CaCO_3$-$Ca_5(PO_4)_3$(Cl,F,OH), which are part of the systems CaO-CO_2-P_2O_5-Cl_2, CaO-CO_2-P_2O_5-F_2, and CaO-CO_2-P_2O_5-H_2O, respectively. Bulk compositions were chosen to investigate a possible effect of halogen (F, Cl) and hydroxyl (OH) substitution in the apatite structure on trace-element partitioning, which was recently suggested by Fleet and Pan (1995, 1997).

Starting materials consisted of mechanical mixes of pure synthetic substances [$CaCO_3$, $Ca_3(PO_4)_2$, CaF_2, $CaCl_2$, and synthetic $Ca_5(PO_4)_3(OH)$]. All chemicals were first dried at 150 °C for four hours to drive off any residual moisture and stored at 110 °C. Starting materials were combined in appropriate proportions (50% apatite – 50% calcite) and ground under ethanol in an agate mortar to produce homogenous mixtures. Because of the nature of the starting materials used in this study, trace elements were added as oxides and carbonates (Table 1), as neither the carbonate nor the phosphate starting material could be vitrified. The resulting mixture was then carefully homogenized in an agate mortar for several hours. The use of mechanical mixes as starting material complicates matters slightly as complete homogenization of the starting material cannot be guaranteed. However, mass-balance calculations for most trace elements indicate relatively good agreement of nominal starting material composition (Table 1) with measured crystal and melt compositions. Moreover, the aforementioned matters will not affect the partitioning of trace elements between apatite and melts as high run temperatures, and extremely mobile melts ensure rapid equilibration during the runs even though the starting material may not have been homogenized completely. Although the experiments were unreversed (like most other trace-element partitioning studies), the overall quality of our partition coefficients are substantiated by several lines of evidence, such as the overall agreement of partition coefficients obtained with two independent analytical techniques, the systematics of partition coefficients when plotted against ionic radius (see below), and homogenous mineral compositions throughout the charge, which provides direct evidence for chemical equilibration (see below).

Table 1. Nominal trace-element composition of starting materials (ppm)

Run	BS19	BS23	BS25
Starting Mix	SMS6	SMS3	SMS5
Composition	$Ca_5(PO_4)_3$-Cl	$Ca_5(PO_4)_3$-OH	$Ca_5(PO_4)_3$-F
Li	50	50	500
Be	300	300	350
B	500	1000	1000
K	150	200	150
Cs	150	5000	500
Rb	500	1500	500
Sr	500	2000	6000
Ba	1000	1000	5000
Y	250	500	1500
Zr	200	200	400
Nb	150	200	500
Hf	500	500	500
Ta	500	500	500
Pb	500	500	10000
Th	750	500	500
U	500	1500	1500
La	1000	1000	1500
Ce	1000	500	1000
Pr	1000	1000	1500
Sm	1000	1000	1500
Gd	500	2500	2500
Lu	500	1000	1000

Experimental techniques

High-pressure high-temperature experiments were carried out in a conventional 1.27 cm piston-cylinder apparatus at the University of Bristol. Experimental techniques are identical to those reported in Klemme et al. (2002). The pressure assembly consists of two inner parts of alumina surrounded by concentric shells of a graphite heater, a soft glass tube of Pyrex, and an outermost sleeve of NaCl, pressed to >95% of the theoretical density. This low-friction assembly requires only a small friction correction of –3% (Brodholt and Wood 1994). The starting materials were sealed into platinum capsules, which were placed in holes in the lower alumina inner part, and separated from the thermocouple by a 0.5 mm Al_2O_3 disc. The runs were performed using the "hot piston-in" routine. First, a pressure of ~0.25 GPa was applied. Then, the sample was heated up to 500 °C to soften the glass. During compression to the final run conditions, pressure and temperature were raised simultaneously. Pressure was kept constant during runs to within ±0.05 GPa, by manual adjustment if necessary. All experiments were run at a pressure of 1 GPa and a temperature of 1250 °C. Temperature was measured with a calibrated $W_{95}Re_5$-$W_{75}Re_{25}$ thermocouple inserted axially into the assembly using four-bore high-purity Al_2O_3 tubing. No corrections were applied to correct for the effect of pressure on the thermocouple EMF. The sample was placed in the hotspot of the assembly, and temperature uncertainties are estimated to be less than 15 °C. Run durations and experimental run conditions are listed in Table 2.

Analytical techniques

The experimental run products were sectioned longitudinally with a diamond saw, and one half was mounted in epoxy and carefully polished with sandpaper, followed by a series of oil-based diamond pastes. Run products were carbon-coated for electron microprobe analysis and gold-coated for ion microprobe analysis. Apatite crystals were generally 50–150 μm

in size, whereas carbonatite melts quenched to sub-micrometer crystals (<1 μm). Major-element concentrations were determined by wavelength-dispersive electron microprobe analysis on a 4-spectrometer JEOL 8600 electron microprobe at the University of Bristol, using a 15 kV-accelerating potential and a beam current of 10 nA. Quenched melts were analyzed with a 5 μm diameter beam calibrated on mineral standards such as apatie and calcite.

All experiments were analyzed for trace elements by secondary ion mass spectrometry (SIMS) using a Cameca ims 4f ion microprobe at the University of Edinburgh. The primary beam consisted of $^{16}O^-$ at a nominal accelerating potential of 10.7 kV and a beam current of 10 nA, resulting in a sputtering surface ~25 μm in diameter. Positive secondary ions were accelerated to 4.5 keV, with an offset of 75 eV to reduce the transmission of molecular ion species. The energy window was set at 25eV. The following masses were counted: ^{7}Li, ^{9}Be, ^{11}B, ^{30}Si, ^{31}P, ^{39}K, ^{42}Ca, ^{47}Ti, ^{85}Rb, ^{88}Sr, ^{89}Y, ^{90}Zr, ^{93}Nb, ^{133}Cs, ^{138}Ba, ^{139}La, ^{140}Ce, ^{141}Pr, ^{149}Sm, ^{160}Gd, ^{175}Lu, ^{178}Hf, ^{181}Ta, ^{208}Pb, ^{232}Th, ^{238}U, and ratioed to ^{42}Ca**,** after calibration on NIST standard SRM 610. Note that Si (cf., Table 2), which was not doped, must have been introduced to the starting materials during grinding in the agate mortar. Mass 130.5 was used to monitor the background; all analyses reported here have zero background counts. Replicate analyses of in-house standards KH-1 (cf., van Westrenen et al. 1999) over a 6-year period (e.g., Blundy and Dalton 2000) demonstrate that calibration on SRM-610 yielded results for a wide range of trace elements that are accurate to better than ±20% (relative). Typical analytical precision is estimated better than 10% (relative) for all elements in apatite and quenched melts. Contamination of crystal analyses by surrounding matrix material is not a problem here as crystal size is much larger than the diameter of the ion beam. Note that some of the scatter in the melt analyses (Table 2) may be caused during the quench, as these carbonatite melts could not be quenched to glass.

To cross-check the ion microprobe measurements, all three run products also were analyzed for trace elements using laser ablation ICP-MS techniques at the University of Bristol. The LA-ICP-MS system consisted of a LUV266X laser (New Wave Research Inc., USA) linked to a PlasmaQuad3 with a supplement rotary pump attached to its interface (the so-called *S*-op-

TABLE 2. Experimental run conditions, major- and trace-element composition of apatites and carbonatite melts

Run	BS19			BS23			BS25		
	P (GPa) 1.0 ± 0.05	*T* (°C) 1250 ± 15	Time (h) 42	*P* (GPa) 1.0 ± 0.05	*T* (°C) 1250 ± 15	Time (h) 92	*P* (GPa) 1.0 ± 0.05	*T* (°C) 1250 ± 15	Time (h) 45
Major elements									
	apatite	melt		apatite	melt		apatite	melt	
SiO_2	0.4(1)	0.5(1)		0.3(1)	0.6(4)		0.2(1)	0.5(3)	
Al_2O_3	n.d.	n.d.		n.d.	0.03(3)		0.1(1)	n.d.	
CaO	53.6(2)	54.0(28)		54.1(2)	53.5(26)		53.5(4)	53.8(19)	
P_2O_5	40.1(3)	7.4(11)		41.1(3)	8.1(21)		40.8(3)	7.9(19)	
FeO	0.01(2)	0.02(1)		0.02(2)	0.04(3)		n.d.	n.d.	
SrO	0.05(2)	0.10(3)		0.20(3)	0.44(5)		0.10(5)	0.3(2)	
Na_2O	0.14(2)	0.6(3)		0.12(3)	0.5(3)		0.10(4)	0.5(2)	
F	0.8(2)	0.6(2)		0.5(1)	0.2(1)		4.3(3)	3.1(12)	
Cl	4.1(2)	2.1(7)		0.7(1)	0.4(1)		0.2(1)	0.3(2)	
Total	99.1	65.3		97.0	63.8		99.3	66.4	
Trace elements									
	apatite (4)	melt (5)	D Apt/Cbt	apatite (3)	melt (5)	D Apt/Cbt	apatite (3)	melt (8)	D Apt/Cbt
Li	11.4(8)	260(70)	0.044(12)	16.8(13)	370(80)	0.046(11)	8.2(2)	830(870)	0.010(10)
Be	0.8(3)	1600(700)	0.0005(3)	0.8(1)	150 (800)	0.0006(3)	0.15(1)	680(1100)	0.0002(4)
B	13.7(11)	1100(600)	0.013(7)	200(10)	4060(730)	0.049(9)	37.9(19)	1930(1430)	0.020(15)
Si	2200(150)	2400(200)	0.89(10)	1048(14)	3040(1100)	0.35(12)	1280(40)	1770(1010)	0.73(42)
K	6.5(11)	290(80)	0.022(7)	11.0(28)	410(100)	0.03(1)	4.0(3)	260(130)	0.016(8)
Rb	7.2(32)	1300(400)	0.006(3)	13.5(4)	2640(510)	0.010(1)	1.6(2)	1240(790)	0.001(1)
Sr	361(3)	862(40)	0.42(2)	1485(15)	3510(140)	0.42(2)	4450(40)	15700(8400)	0.28(15)
Y	198(11)	395(37)	0.50(5)	390(190)	920(50)	0.42(21)	1010(30)	2750(1170)	0.37(16)
Zr	15(1)	560(280)	0.026(13)	8.1(29)	880(120)	0.009(4)	7.1(1)	1260(710)	0.006(3)
Nb	2.8(1)	590(300)	0.005(2)	7(3)	1050(175)	0.007(3)	4.0(5)	1660(900)	0.002(1)
Cs	3.4(24)	780(280)	0.004(3)	11.9(61)	27500(19150)	0.0004(4)	0.4(1)	1370(790)	0.0003(2)
Ba	25(3)	2160(1930)	0.012(11)	135(23)	4920(2170)	0.027(13)	167(3)	11500(4000)	0.015(5)
La	570(30)	1720(80)	0.33(2)	640(40)	2760(120)	0.23(2)	850(15)	3000(890)	0.28(8)
Ce	630(30)	1570(80)	0.40(3)	140(80)	430(50)	0.33(20)	410(13)	2210(1290)	0.19(11)
Pr	820(40)	1820(120)	0.45(4)	770(40)	2500(100)	0.31(2)	1130(20)	3060(1020)	0.37(12)
Sm	810(50)	1480(140)	0.55(6)	960(240)	2260(80)	0.43(11)	1160(30)	2580(860)	0.45(15)
Gd	640(30)	1100(100)	0.58(6)	2070(240)	4010(180)	0.52(19)	2110(50)	4290(1460)	0.49(17)
Lu	460(30)	1400(260)	0.33(7)	430(290)	1270(100)	0.34(23)	640(20)	2820(1180)	0.23(10)
Hf	10.1(8)	590(390)	0.017(11)	2.2(2)	390(50)	0.006(1)	2.2(2)	630(300)	0.004(2)
Ta	5.1(6)	790(490)	0.006(4)	6.5(29)	510(85)	0.013(6)	2.3(5)	420(220)	0.006(3)
Pb	29(9)	78(19)	0.37(15)	860(40)	64000(79000)	0.013(16)	800(20)	50000(95000)	0.02(3)
Th	540(40)	1330(710)	0.41(22)	69(25)	275(30)	0.25(9)	160(5)	1200(570)	0.13(6)
U	85(17)	760(480)	0.11(7)	2.2(7)	3290(290)	0.0007(2)	1.15(10)	4200(2000)	0.0003(1)

Notes: Major element compositions of apatites and quenched melts were analyzed with the electron microprobe (wt%). Note that Mg and Mn were also analyzed but could not be detected in any run product. Trace element composition of apatites and quenched carbonatite melts were determined by secondary ion mass spectrometry (ppm). Number of analyses are given in brackets. Also given are calculated partition coefficients (*D* Apt/Cbt). Standard deviations of analyses quoted in terms of last significant digits (1σ). Also given are experimental run conditions of each experiment. Abbreviations: *P* = pressure (GPa), *T* = temperature (°C), Time = run duration (hours).

tion, Thermo Elemental, UK). For detailed information on parameters used see Table 3. For each analysis, 22 isotopes were measured repetitively in the mass spectrometer for a total time of 60 s. The first 15 seconds of acquisition were used to measure the gas blank followed by about 45 seconds of acquiring a mixture of gases and ablated materials. The gas mixture used during each analysis consisted of pure He (Grade 5.9 from Air Products, UK), which was used in the sample cell and later mixed downstream with pure Ar (Grade 5 from BOC, UK) using a Y-connector located 15 cm away from the sample cell. The laser beam was condensed with a beam expander and shaped with an adjustable iris aperture to produce a crater size of ~35 µm on the sample surface. The internal isotope standard used was ^{44}Ca, which successfully reproduces the trace-element concentrations of NIST SRM 610 and 612 glasses within a relative difference of ±10% or less from published values (Pearce et al. 1997).

Figure 1 compares calculated partition coefficients (D-values) obtained by ion microprobe technique (SIMS) to those obtained by laser ablation ICP-MS (Table 4). We find reasonable agreement for most elements, with notable exceptions being Be and Pb, the partition coefficients of which are generally of poor quality. Mass-balance calculations indicate either a significant Pb loss to the capsule material (which should not affect the partitioning), or matrix effects during SIMS analysis that were not accounted for during data reduction. Therefore, Pb and Be partition coefficients should only be used with caution. However, the relatively good agreement of partition coefficients for most other elements (within the uncertainties) indicates generally good agreement of both analytical techniques (Fig. 1).

Results and discussion

The experimental run products contained apatite crystals and a quenched carbonatite-melt. Apatites were generally between 50 to 100 µm across, with no significant zonation or inclusions. The quenched carbonatite melt consisted of a very-fine intergrowth of unidentifiable, submicrometer crystals. Melts contained about 7–8 wt% P_2O_5, in good agreement with the data of Baker and Wyllie (1992), albeit for different bulk compositions. Table 2 lists the major- and trace-element compositions of apatites, quenched carbonatite melt, and calculated partition coefficients for each experiment. These are the first published experimental partition coefficients between apatite and carbonatite melt.

Figure 2 depicts partition coefficients between apatite and carbonatite melts. Most elements are incompatible in apatite (i.e., $D < 1$). Beryllium, Cs, and Rb are most incompatible whereas the REE are near to compatible in apatite. Partition coefficients for REE uniformly show a convex-upward shape, as apatite accommodates the middle REE more readily than the light or the heavy REE. D_{Lu} are roughly similar to D_{La}. Other interesting findings are that Li^+ and B^{3+} are significantly more compatible than Be^{2+}, whereas Th^{4+} is significantly more compatible than U^{4+}. Partition coefficients of the high field-strength elements (HFSE) are of similar magnitude, with D_{Nb} slightly lower than D_{Ta}, and D_{Zr} slightly higher than D_{Hf}. As our experiments were unbuffered in respect to oxygen fugacity, some oxidation of U^{4+} to U^{6+} may have occurred, which could explain the rather low D_U in BS 23 and BS25.

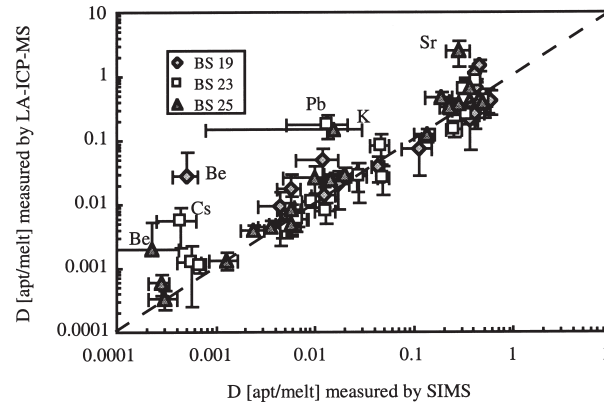

Figure 1. Comparison of partition coefficients obtained by secondary ion mass spectrometry (SIMS) and by laser ablation ICP-MS (LA-ICPMS), respectively. Relatively good agreement is found for most measured trace elements (within the uncertainties), with some notable exemptions (Be, Pb, K, Cs in BS 23 and Sr in BS 25; see text for further discussion). Error bars represent one standard deviation (1σ).

Table 3. Laser and ICP-MS operating conditions

Laser	
Energy	0.06 ± 0.02 mJ
Frequency	5 Hz
Optical attenuator	100% opening
Cell gas (flow rate)	He (0.25–0.31 l/min)
Mixing gas (flow rate)	Ar (1.02–1.13 l/min)
ICP-MS	
Cooling gas	13.5 l/min
Auxiliary gas	0.8–0.9 l/min
Acquisition mode	peak jumping in time resolved analysis
Quad settle time	10 ms
Measuring point / mass	1
Dwell time per point (Mass analyzed)	15 ms (^{7}Li, ^{9}Be, ^{11}B, ^{44}Ca, ^{85}Rb, ^{88}Sr, ^{89}Y, ^{90}Zr, ^{93}Nb, ^{133}Cs, ^{137}Ba, ^{139}La, ^{140}Ce, ^{141}Pr, ^{147}Sm, ^{157}Gd, ^{175}Lu, ^{178}Hf, ^{181}Ta, ^{208}Pb, ^{232}Th, ^{238}U)

Table 4. Partition coefficients calculated from laser ablation ICP-MS analyses

	Li	Be	B	Rb	Sr	Y
BS19	0.039(32)	0.028(38)	0.014(5)	0.018(12)	0.652(231)	0.37(15)
BS23	0.084(41)	0.001(1)	0.027(13)	0.004(1)	0.824(49)	0.4(7)
BS25	0.027(12)	0.002(3)	0.030(8)	0.0010(5)	2.4(10)	0.42(5)
	Zr	Nb	Cs	Ba	La	Ce
BS19	0.030(14)	0.005(2)	0.009(7)	0.051(26)	0.74(19)	1.1(3)
BS23	0.011(3)	0.006(2)	0.006(3)	0.028(17)	0.31(4)	0.4(1)
BS25	0.008(2)	0.004(1)	0.0003(1)	0.025(3)	0.37(7)	0.49(7)
	Pr	Sm	Gd	Lu	Hf	Ta
BS19	1.5(3)	0.4(2)	0.4(2)	0.70(19)	0.02(1)	0.006(2)
BS23	0.63(6)	0.42(8)	0.41(9)	0.25(7)	0.008(5)	0.008(3)
BS25	0.6(1)	0.44(7)	0.39(5)	0.34(6)	0.004(1)	0.005(2)
	Pb	Th	U			
BS19	0.21(14)	0.2(1)	0.08(5)			
BS23	0.18(7)	0.15(4)	0.0010(3)			
BS25	0.15(3)	0.12(3)	0.0010(5)			

Standard deviations of analyses quoted in terms of last significant digits.

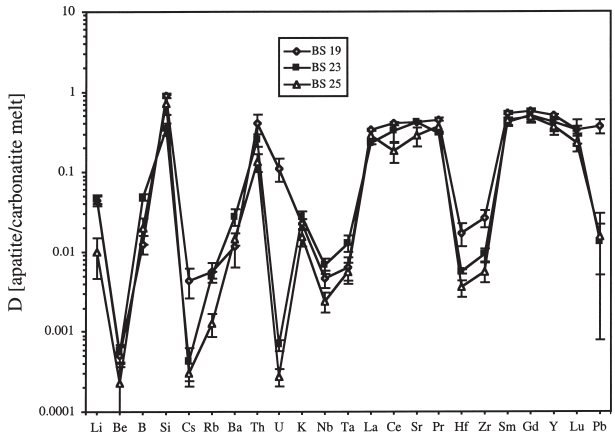

FIGURE 2. Experimentally determined trace element partition coefficients between apatite and carbonatite melt, in three different bulk compositions: BS19 (chlorapatite), BS23 (hydroxylapatite), BS25 (fluorapatite). We observe only small differences between the rare-earth element partition coefficients. Note that D_U, D_{Cs}, D_{Pb}, and perhaps D_{Zr} and D_{Hfi}, are somewhat higher for run BS 19 than for the other experiments.

The crystal structure of apatite

Fluorapatite [$Ca_5(PO_4)_3F$)], which is the most-common phosphate mineral in carbonatites (Hogarth 1989) and the Earth's crust in general, crystallizes in the hexagonal space group $P6_3/m$ (Bragg et al. 1965). Hydroxylapatite has a modified, but similar structure (Fleet et al. 2000b). For natural chlorapatite, the symmetry is monoclinic with space group $P2_1/a$ (Mackie et al. 1972; Hogarth 1988), but it inverts to a hexagonal form upon heating at 350 °C (Bauer and Klee 1993).

The structure of apatite can be visualized as a series of phosphate "tubes" internally lined by Ca ions. There are two Ca-sites in the apatite structure (Mackie and Young 1973, Fleet and Pan 1995; Hughes et al. 1989, 1991). This is of importance here as REE substitute for Ca^{2+} in the apatite structure (e.g., Hughes et al. 1991). Calcium ions on the A1 site [referred to as Ca1 in some previous studies; e.g., Hughes et al. (1991)] are closely surrounded by six neighboring oxygen atoms, further coordinated by three oxygen atoms at greater distance. The second Ca site (i.e., *A*2 or *Ca*2 as referred by previous studies) is half-surrounded by six oxygen atoms, and half-exposed to the central space into which the anions such as F^-, Cl^-, or OH^- are located. Hughes et al. (1991) showed that the *A*1 position may be approximated by a distorted ninefold coordination; the lattice energy on *A*1, however, is dominated by a sixfold coordination of Ca (average <Ca-O> bond distance ~2.4-2.5 Å), with only small contributions expected from oxygen atoms in greater bond distance (average <Ca-O3> bond distance ~2.8 Å; Fleet et al. 2000a). The A2 position in apatite may be described as sevenfold coordinated (Hughes et al. 1991), although lattice energetics are expected to be dominated by contributions of six oxygen atoms octahedrally coordinating the Ca on *A*2, with probably only a small influence of the anion at greater distance.

Crystal-chemical controls on REE site occupancy in apatites are controversial. This subject has recently been discussed by Hughes et al. (1991) and by Fleet and coworkers (Fleet and Pan 1995, 1997; Fleet et al. 2000a, 2000b). Crystallographic results by Hughes et al. (1991) showed preference of the lighter REE (La^{3+}-Pr^{3+}) for the *A*2 position, whereas heavier REE (i.e., Sm^{3+}-Lu^{3+}) seemed to prefer the *A*1 position. This result was questioned somewhat by Fleet and co-workers (e.g., Fleet and Pan 1995, 1997; Fleet et al. 2000b), who found a general preference of all REE for the *A*2 site in synthetic hydroxyl- and fluorapatites. Synthetic chlorapatites, however, seemed to concentrate the REE (La^{3+}-Dy^{3+}) on *A*1 rather than the *A*2 site (Fleet et al. 2000a). Some older studies indicated no particular preference of the REE for either site (Cockbain and Smith 1967; Mackie and Young 1973). Nevertheless, a crystal-chemical control on REE uptake is consistent with a generally observed, upward-convex pattern for the REE in apatite (Fleet and Pan 1995, 1997; Sha and Chappell 1999), indicating preferential uptake of Nd^{3+} relative to La^{3+} or Lu^{3+} in the apatite structure. Moreover, Fleet and Pan (1997) speculated that the volatile anion component (i.e., Cl^-, F^-, or OH^-) might play an important role in the trace-element uptake of apatite because of its proposed influence of the stereochemical environment and the size of the *A*2-site. Our new partition coefficients for the REE may shed some new light on these problems.

Interpretation with the lattice strain model

For interpretation of partition coefficients, the lattice-strain model (Brice 1975; Blundy and Wood 1994; Wood and Blundy 1997) recently has been employed successfully for a number of phases. The lattice-strain model is based on the observation that partition coefficients follow a near-parabolic trend when plotted against ionic radius (e.g., Onuma et al. 1968). In the model of Blundy and Wood (1994), trace-element partitioning on a given structural site is characterized by the ionic radius (r_i), its Young's modulus (E), and the strain-free partition coefficient D_0 for an element with an ideal radius r_0:

$$D_i = D_0 \cdot \exp\left[\frac{-4\pi E N_A\left[\frac{r_0}{2}(r_i - r_0)^2 + \frac{1}{3}(r_i - r_0)^3\right]}{RT}\right]$$

N_A is Avogadro's number, R is the universal gas constant, and T is the temperature in Kelvin. The lattice strain model works well for garnets (e.g., van Westrenen et al. 1999, Klein et al. 2000), clinopyroxenes (Wood and Blundy 1997; Blundy and Dalton 2000; Hill et al. 2000; Landwehr et al. 2001; Klemme 2001), and amphibole (Brenan et al. 1995; LaTourrette et al. 1995; Tiepolo et al. 2000; Dalpé and Baker 2000), and it also has been employed to interpret wollastonite/melt partitioning (Law et al. 2000). In the case of apatite, however, we encounter the following problems that complicate interpretations using the lattice-strain model. First, following Hughes et al. (1991), two distinct sites (i.e., *A*1 and *A*2) in apatite would require separate analysis of the partitioning of trace elements on each side. This is unfortunate, as interpretation with the lattice-strain model [or, parabolic plots of partition coefficients in so-called "Onuma" diagrams; cf., Onuma et al. (1968)] requires at least four data points per crystallographic site, more

data than we were able to measure. Moreover, our D_{Ce} data seem to be somewhat corrupted, perhaps due to oxidation of Ce^{3+} to Ce^{4+} in some runs. Thus, we assumed sixfold coordination on both Ca-sites, a simplification that may be justified because, in terms of the factors that control partitioning, both Ca-sites are large and will be highly disordered at near-liquidus temperatures, with similar elastic properties (Yoon and Newnham 1969). Moreover, this assumption may be justified due to consistent site partitioning (see below). Non-linear, least-square fitting routines were employed to derive best-fit values (Table 5) for r_0, D_0, and E for the experimentally determined partitioning of the trivalent ions (REE and Y^{3+}, Figs. 3 and 4). Standard deviations of multiple analyses (Table 2) were used to weight the fits assuming that the REE (including Y^{3+}) partition into both Ca-sites of apatite in octahedral coordination, with no particular preference for either site (see above). With the exception of Pr in BS 23, plots of ionic radius vs. experimentally determined partition coefficients (Fig. 4) indicate good agreement between theory and experiment. A more-detailed discussion of apatite melt partitioning on the different Ca-sites with the lattice-strain model requires more data and remains an important task for experimental geochemists.

Fleet et al. (2000a) speculated about the influence of the volatile anion component (Cl^-, F^-, and OH^-) on REE partitioning between apatite and phosphate melts. As our experiments were performed with three different compositions, i.e., with chlorapatite, fluorapatite, and hydroxylapatite, a strong influence of the anion species on the *A*2-site should result in significantly different REE partition coefficients. This is not the case within the analytical uncertainties. We find only very slightly differing REE partition coefficients for the three compositions (Fig. 2 and 4): The highest D_{REE} values were measured for chlorapatite (BS19), followed by hydroxylapatite (BS23), and fluorapatite (BS25).

However, our data clearly show that melt composition exerts a significant influence on REE partition coefficients (Fig. 3, Fig. 5). Similarly, Watson and Green (1981) found decreasing REE partition coefficients with decreasing silica activity in melts, a trend that is confirmed by our apatite/carbonatite melt partition coefficients (Figs. 5 and 6). Partition coefficients decrease with decreasing SiO_2, and increasing CaO and P_2O_5 contents of melts, respectively (Figs. 5 and 6). It is unclear which mechanism exactly controls partitioning in our experiments: It may either be a single melt component that, by some sort of complexation mechanism, enables the melt to attract more trace elements relative to the apatite crystal or it may indeed be a combination of several factors. Recent work by Finch et al. (2001) and Hanchar et al. (2001) have shown for zircon ($ZrSiO_4$) that uptake of the REE critically depends on the presence of P in the melt, as REE are incorporated into the zircon structure by the following substitution mechanism: $Zr^{4+} + REE^{3+} = Si^{4+} + P^{5+}$. In the case of apatite, there are several possible substitution mechanisms, such as $Si^{4+} + REE^{3+} = Ca^{2+} + P^{5+}$ or $Na^+ + REE^{3+} = 2\ Ca^{2+}$ (cf., Cherniak 2000). Therefore, the partitioning of trace elements may depend on the P, Si, or Na activity of the melt, which is in good agreement with our results. The aforementioned mechanisms alone are not sufficient, however, to explain uptake of the REE in our apatites,

TABLE 5. Lattice strain parameters

	BS19	BS23	BS25
E (GPa)	223(28)	321(95)	405(170)
r_0 (Å)	0.943(4)	0.94(1)	0.94(1)
D_0	0.55(2)	0.50(5)	0.47(5)

Notes: Lattice strain parameters derived from parabolic fits to equation (1). Uncertainties are 1SD, expressed in terms of last significant digits. Note that Ce and Pr were excluded from BS 25 and BS 23, respectively.

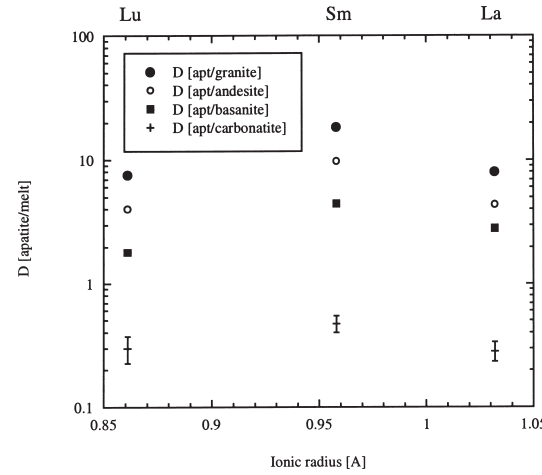

FIGURE 3. Plots of partition coefficients vs. ionic radius, comparing apatite/silicate melt partition coefficients (Watson and Green 1981) for selected REE with our new apatite/carbonatite melt partition coefficients. We observe a strong decrease of all D_{REE} as the silica activity decreases in melts. Partition coefficients of apatite/silicate melt (*D* apt/granitic melt, *D* apt/andesitic melt, *D* apt/basanitic melt) were taken from Watson and Green (1981). Both our new data and those of Watson and Green (1981) indicate a strong influence of melt chemistry on trace-element partitioning (see text for further discussion).

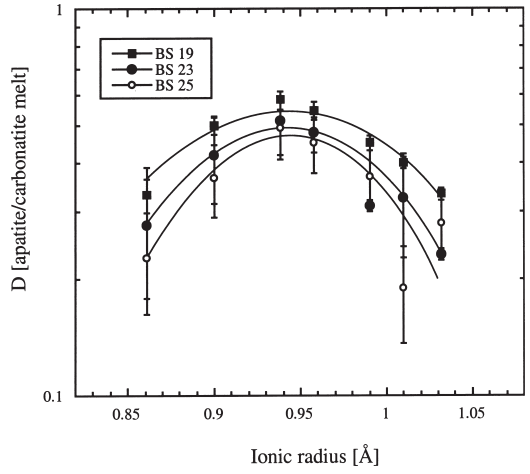

FIGURE 4. Onuma diagrams of partition coefficients plotted vs. ionic radius in sixfold coordination for the REE entering both Ca-sites [ionic radii from Shannon (1976)]. Lines represent weighted non-linear least-squares regressions to Equation 1. Fit parameters are given in Table 5 (see text for further information).

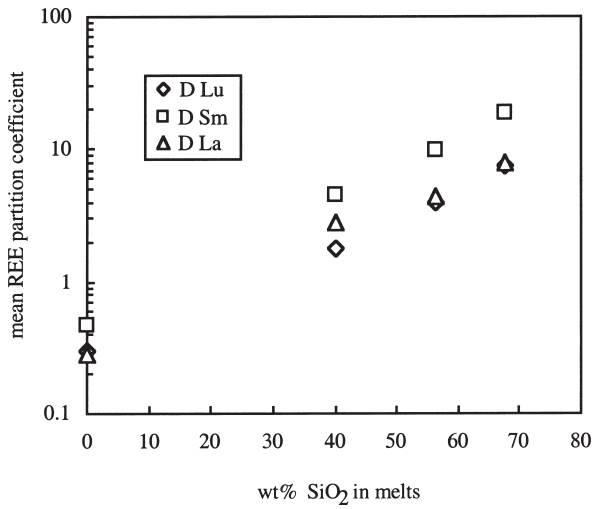

FIGURE 5. The influence of melt composition on REE partitioning. Depicted are partition coefficients between apatite and several different melts [carbonatite melt = virtually no SiO_2 (this study); basanitic melt = 40% SiO_2, andesitic melt =56 % SiO_2, and granitic melt = 68 % SiO_2 (Watson and Green 1981)]. Partition coefficients decrease significantly with decreasing silica activity of melts.

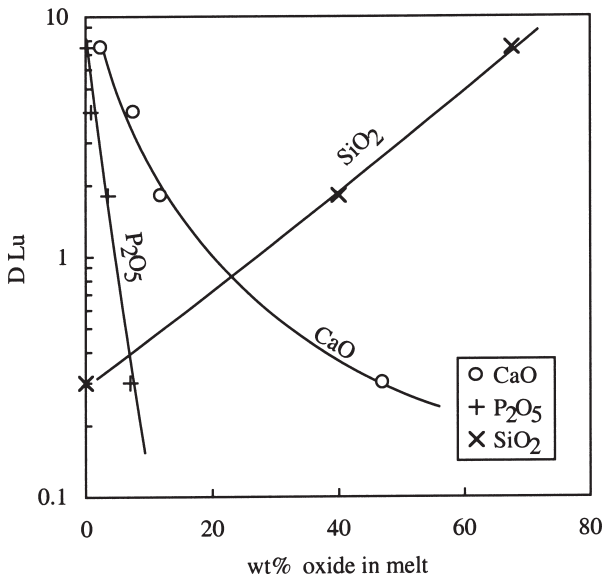

FIGURE 6. The influence of melt composition on REE partition coefficients. Depicted are D_{Lu} as a function of SiO_2, CaO, and P_2O_5 contents of melts, respectively. Partition coefficients are correlated positively with SiO_2, but inversely with CaO and P_2O_5 contents of melts. Data are from Watson and Green (1981) and from this study (i.e., D_{Lu} ~0.3).

and other mechanisms involving coupling with vacancies (e.g., 3 Ca^{2+} = 2REE^{3+} + □) or anions such are CO_3^{2-} may also be important at the high temperatures of our study. Clearly, however, the influence of melt composition (or bulk composition) on trace-element partitioning for a number of minerals needs to be assessed further and cannot be neglected, especially when minerals crystallize from melts of very different compositions, as is the case for apatite and a number of other accessory phases.

ACKNOWLEDGMENTS

S.K. acknowledges generous funding by the Europeans Union as a Marie-Curie Individual Fellow. C.D. was supported by the EU Large Scale Geochemical Facility. We are grateful to J. Craven and R. Hinton for their help with the SIMS analyses. Many thanks to J. Blundy and B.J. Wood for supporting the LA-ICP-Ms facility. We also thank P. Boyd, M. Dury, and F. Wheeler for technical support with the laser ablation sample cell modifications. Discussions with J. Dalton and many others at Bristol and Heidelberg were of great value. We much appreciated the thorough reviews of D. Musselwhite and A. Treiman, which helped to improve the manuscript significantly.

REFERENCES CITED

Baker, M.B. and Wyllie, P.J. (1992) High-pressure apatite solubility in carbonate-rich liquids: implications for mantle metasomatism. Geochimica et Cosmochimica Acta, 56, 3409–3422.

Bauer, M. and Klee, W.E. (1993) The monoclinic-hexagonal phase transition in chlorapatite. European Journal of Mineralogy, 5, 307–316.

Biggar, G.M. (1966) Phase relations in the join $Ca(OH)_2$-$CaCO_3$-$Ca_3(PO_4)_2$-H_2O at 1000 bars. Mineralogical Magazine, 35, 75–82.

Blundy, J.D. and Dalton, J.A. (2000) Experimental comparison of trace element partitioning between clinopyroxene and melt in carbonate and silicate systems, and implications for mantle metasomatism. Contributions to Mineralogy and Petrology, 139, 356–371.

Blundy, J.D. and Wood, B.J. (1994) Prediction of crystal-melt partition coefficients from elastic moduli. Nature, 372, 452–454.

Boettcher, A.L., Robertson, J.K., and Wyllie, P.J. (1980) Studies in synthetic carbonatite systems: solidus relationships for CaO-MgO-CO_2-H_2O to 40 kbar and CaO-MgO-SiO_2-CO_2-H_2O to 10 kbar. Journal of Geophysical Research, 85, 6937–6943.

Bragg, L., Claringbull, G.F., and Taylor, W.H. (1965) Crystal structures of minerals. Bell and Sons, London.

Brenan, J.M., Shaw, H.F., Ryerson, F.J., and Phinney, D.L. (1995) Experimental determination of trace element partitioning between pargasitic amphibole and a synthetic hydrous andesitic melt. Earth and Planetary Science Letters, 135, 1–11.

Brice, J.C. (1975) Some thermodynamic aspects of the growth of strained crystals. Journal of Crystal Growth, 28, 249–253.

Brodholt, J.P. and Wood, B.J. (1994) Measurement of the PVT properties of water to 25 kbars and 1600 °C from synthetic fluid inclusions in corundum. Geochimica et Cosmochimica Acta, 58, 2143–2148.

Bühn, B., Wall, F., and Le Bas, M.J. (2001) Rare-earth element systematics of carbonatitic fluorapatites, and their significance for carbonatite magma evolution. Contributions to Mineralogy and Petrology, 141, 572–591.

Cherniak, D.J. (2000) Rare earth element diffusion in apatite. Geochimica et Cosmochimica Acta, 64, 3871–3885.

Cockbain, A.G. and Smith, G.V. (1967) Alkaline-earth rare-earth silicate and germanate apatites. Mineralogical Magazine, 36, 411–421.

Coltorti, M., Bonadiman, C., Hinton, R.W., Siena, F., and Upton, B.G.J. (1999) Carbonatite metasomatism of the oceanic upper mantle: Evidence from clinopyroxenes and glasses in ultramafic xenoliths of Grande Comore, Indian Ocean. Journal of Petrology, 40, 133–165.

Dalpé, C. and Baker, D.R. (2000) Experimental investigation of large-ion-lithophile-element-, high-field-strength-element- and rare-earth-element-partitioning between calcic amphibole and basaltic melt: the effects of pressure and oxygen fugacity. Contributions to Mineralogy and Petrology, 140, 233–250.

Elliott, T., Plank, T., Zindler, A., White, W., and Bourdon, B. (1997) Element transport from slab to volcanic front at the Mariana arc. Journal of Geophysical Research, 102, 14991–15019.

Eriksson, S.C. (1989) Phalaborwa: a saga of magmatism, metasomatism, and miscibility. In K. Bell, Ed., Carbonatites - Genesis and Evolution, p. 221–254. Unwin Hyman, London.

Finch, R.J., Hanchar, J.M., Hoskin, P.W.O., and Burns, P.C. (2001) Rare earth elements in synthetic zircon: Part 2. A single crystal X-ray study of xenotime substitution. American Mineralogist, 86, 681–689.

Fleet, M.E. and Pan, Y. (1995) Site preference of rare earth elements in fluorapatite. American Mineralogist, 80, 329–335.

——— (1997) Rare earth elements in apatite: uptake from H_2O-bearing phosphate fluoride melts and the role of volatile components. Geochimica et Cosmochimica Acta, 61, 4745–4760.

Fleet, M.E., Liu, X., and Pan, Y. (2000a) Rare earth elements in chlorapatite [$Ca_{10}(PO_4)_6Cl_2$]:Uptake, site preference, and degradation of monoclinic structure. American Mineralogist, 85, 1437–1446.

——— (2000b) Site preference of rare earth elements in hydroxyapatite [$Ca_{10}(PO_4)_6(OH)_2$]. Journal of Solid State Chemistry, 149, 391–398.

Frey, F.A. and Green, D.H. (1974) The mineralogy, geochemistry, and origin of lherzolite inclusions in Victorian basanites. Geochimica et Cosmochimica Acta, 38, 1023–1059.
Green, D.H. and Wallace, M.E. (1988) Mantle metasomatism by ephemeral carbonatite melts. Nature, 336, 459–462.
Green, T.H. (1994) Experimental studies of trace-element partitioning applicable to igneous petrogenesis - Sedona 16 years later. Chemical Geology, 117, 1–36.
Haggerty, S.E., Fung, A.T., and Burt, D.M. (1994) Apatite, phosphorus and titanium in eclogitic garnet from the upper mantle. Geophysical Research Letters, 21(16), 1699–1702.
Hanchar, J.M., Finch, R.J., Hoskin, P.W.O., Watson, E.B., Cherniak, D.J., and Mariano, A.N. (2001) Rare earth elements in synthetic zircons: Part 1. Synthesis, and rare-earth element and phosphorus doping. American Mineralogist, 86, 667–680.
Harrison, T.M. and Watson, E.B. (1984) The behavior of apatite during crustal anatexis: Equilibrium and kinetic considerations. Geochimica et Cosmochimica Acta, 48, 1467–1477.
Hill, E., Wood, B.J., and Blundy, J.D. (2000) The effect of Ca-Tschermaks component on trace element partitioning between clinopyroxene and silicate melt. Lithos, 53, 203–215.
Hogarth, D.D. (1988) Chemical composition of fluorapatite and associated minerals from skarn near Gatineau, Quebec. Mineralogical Magazine, 52, 347–358.
——— (1989) Pyrochlore, apatite and amphibole: distinctive minerals in carbonatite. In K. Bell, Ed., Carbonatites—Genesis and Evolution, p. 105–148. Unwin Hyman, London.
Hoskin, P.W.O., Kinny, P.D., Wyborn, D., and Chappell, B.W. (2000) Identifying accessory mineral saturation during differentiation in granitoid magmas: an integrated approach. Journal of Petrology, 41, 1365–1396.
Hughes, J.M., Cameron, M., and Crowley, K.D. (1989) Structural variations in natural F, OH, and Cl apatites. American Mineralogist, 74, 870–876.
Hughes, J.M., Cameron, M., and Mariano, A.N. (1991) Rare-earth element ordering and structural variations in natural rare-earth-bearing apatites. American Mineralogist, 76, 1165–1173.
Ionov, D.A., Dupuy, C., O'Reilly, S.Y., Kopylova, G.M., and Genshaft, Y.S. (1993) Carbonated peridotitic xenoliths from Spitsbergen: implications for trace element signature of mantle carbonate metasomatism. Earth and Planetary Science Letters, 119, 283–297.
Ionov, D.A., Hofmann, A.W., and Shimizu, N. (1994) Metasomatism-induced melting in mantle xenoliths from Mongolia. Journal of Petrology, 35, 753–785.
Ionov, D.A., Griffin, W.L., and O'Reilly, S.Y. (1997) Volatile-bearing minerals and lithophile trace elements in the upper mantle. Chemical Geology, 141, 153–184.
Klein, M., Stosch, H.G., Seck, H.A., and Shimizu, N. (2000) Experimental partitioning of high field strength elements between clinopyroxene and garnet in andesitic to tonalitic systems. Geochimica et Cosmochimica Acta, 64, 99–115.
Klemme, S. (2001) Experimentally determined trace element partitioning between baddeleyite and carbonatite melts. Journal of Conference Abstracts, 6, 491.
Klemme, S., van der Laan, S.R., Foley, S.F., and Günther, D. (1995) Experimentally determined trace and minor element partitioning between clinopyroxene and carbonatite melt under upper mantle conditions. Earth and Planetary Science Letters, 133, 439–448.
Klemme, S., Blundy, J.D., and Wood, B.J. (2002) Experimental constraints on major and trace element partitioning during partial melting of eclogite. Geochimica et Cosmochimica Acta, 66:3109–3123.
Landwehr, D., Blundy, J., Chamorro-Perez, E.M., Hill, E., and Wood, B.J. (2001) U-series disequilibria generated by partial melting of spinel lherzolite. Earth Planetary Science Letters, 188, 329–348.
LaTourrette, T.Z., Hervig, R.L., and Holloway, J.R. (1995) Trace element partitioning between amphibole, phlogopite, and basanitic melt. Earth and Planetary Science Letters, 135, 13–30.
Law, K.M., Blundy, J.D., Wood, B.J., and Ragnarsdottir, K.V. (2000) Trace element partitioning between wollastonite and silicate-carbonate melt. Mineralogical Magazine, 64, 651–661.
Mackie, P.E. and Young, R.A. (1973) Location of Nd dopant in fluorapatite, $Ca_5(PO_4)_3F$:Nd. Journal of Applied Crystallography, 6, 26–31.
Mackie, P.E., Elliott, J.C., and Young, R.A. (1972) Monoclinic structure of synthetic $Ca_5(PO_4)_3Cl$, chlorapatite. Acta Crystallographica, B28, 1840–1848.
Matsumoto, T., Honda, M., McDougall, I., and Yatsevich, I. (1997) Primitive and nucleogenic neon in a metasomatic apatite in a mantle xenolith from Australia. Nature, 388, 162–164.
Nichols, G.T., Wyllie, P.J., and Stern, C.R. (1994) Subduction zone melting of pelagic sediments constrained by melting experiments. Nature, 371, 785–788.
O'Reilly, S.Y. and Griffin, W.L. (2000) Apatite in the mantle: implications for metasomatic processes and high heat production in Phanerozoic mantle. Lithos, 53, 217–232.
Onuma, N., Higuchi, H., Wakita, H., and Nagasawa, H. (1968) Trace element partitioning between two pyroxenes and the host lava. Earth and Planetary Science Letters, 5, 47–51.
Pearce, N.J.G., Perkins, W.T., Westgate, J.A., Gorton, M.P., Jackson, S.E., Neal, C.R., and Chenery, S.P. (1997) A compilation of new and published major and trace element data for NIST SRM 610 and NIST SRM 612 glass reference material. Geostandards Newsletter: The Journal of Geostandards and Geoanalysis, 21, 115–144.
Plank, T. and Langmuir, C.H. (1993) Tracing trace elements from sediment input to volcanic output at subduction zones. Nature, 362, 739–742.
——— (1998) The chemical composition of subducting sediment and its consequences for the crust and mantle. Chemical Geology, 145, 325–394.
Rosenbaum, J.M., Wilson, M., and Condliffe, E. (1997) Partial melts of subducted phosphatic sediments in the mantle. Geology, 25, 77–80.
Ryabchikov, I.D., Edgar, A.D., and Wyllie, P.J. (1991) Partial melting in a carbonate-phosphate-peridotite system at 30 kbar. Geokhimiya, 2, 163–168.
Seifert, W., Kampf, H., and Wasternack, J. (2000) Compositional variation in apatite, phlogopite and other accessory minerals of the ultramafic Delitzsch complex, Germany: implication for cooling history of carbonatites. Lithos, 53, 81–100.
Sha, L.-K. and Chappell, B.W. (1999) Apatite chemical composition, determined by electron microprobe and laser ablation inductively coupled plasma mass spectrometry, as a probe into granite petrogenesis. Geochimica et Cosmochimica Acta, 63, 3861–3881.
Shannon, R.D. (1976) Revised effective ionic radii and systematic studies of interatomic distances in halides and chalcogenides. Acta Crystallographica, 32, 751–767.
Sorensen, S.S. and Grossman, J.N. (1993) Accessory minerals and subduction metasomatism: a geochemical comparison of two melanges (Washington and California, U.S.A.). Chemical Geology, 110, 269–297.
Tiepolo, M., Vannucci, R., Oberti, R., Foley, S., Bottazzi, P., and Zanetti, A. (2000) Nb and Ta incorporation and fractionation in titanian pargasite and kaersutite: crystal-chemical constraints and implications for natural systems. Earth and Planetary Science Letters, 176, 185–201.
Van Westrenen, W., Blundy, J.D., and Wood, B.J. (1999) Crystal-chemical controls on trace element partitioning between garnet and anhydrous silicate melt. American Mineralogist, 84, 838–847.
Watson, E.B. and Green, T.H. (1981) Apatite/liquid partition coefficients for the rare-earth elements and strontium. Earth and Planetary Science Letters, 56, 405–421.
Wood, B.J. and Blundy, J.D. (1997) A predictive model for rare earth element partitioning between clinopyroxene and anhydrous silicate melt. Contributions to Mineralogy and Petrology, 129, 166–181.
Yaxley, G.M. and Kemenetsky, V. (1999) In situ origin for glass in mantle xenoliths from southeastern Australia: insights from trace element compositions of glasses and metasomatic phases. Earth and Planetary Science Letters, 172, 97–109.
Yaxley, G.M., Crawford, A.J., and Green, D.H. (1991) Evidence for carbonatite metasomatism in spinel peridotite xenoliths from western Victoria, Australia. Earth and Planetary Science Letters, 107, 305–317.
Yaxley, G.M., Green, D.H., and Kamenetsky, V. (1998) Carbonatite metasomatism in the southeastern Australian lithosphere. Journal of Petrology, 39, 1917–1930.
Yoon, H.S. and Newnham, R.E. (1969) Elastic properties of fluorapatite. American Mineralogist, 54, 1193–1197.
Zaitsev, A. and Bell, K. (1995) Sr and Nd isotope data of apatite, calcite and dolomite as indicators of source, and the relationships of phoscorites and carbonatites from the Kovdor massif, Kola-Peninsula, Russia. Contributions to Mineralogy and Petrology, 121, 324–335.

MANUSCRIPT RECEIVED OCTOBER 29, 2001
MANUSCRIPT ACCEPTED DECEMBER 22, 2002
MANUSCRIPT HANDLED BY JOHN H. JONES